Spectrochimica Acta Part A: Molecular and Biomolecular Spectroscopy 210 (2019) 251–259

Contents lists available at ScienceDirect

Spectrochimica Acta Part A: Molecular and Biomolecular Spectroscopy

journal homepage: www.elsevier.com/locate/saa

A colorimetric paper sensor for citrate as biomarker for early stage detection of prostate cancer based on peroxidase-like activity of cysteine-capped gold nanoclusters

Shima Abarghoei [a], Neda Fakhri [b], Yasaman Sadat Borghei [a], Morteza Hosseini [a,*], Mohammad Reza Ganjali [c,d]

[a] Department of Life Science Engineering, Faculty of New Sciences & Technologies, University of Tehran, Tehran, Iran
[b] School of Chemical Engineering, College of Engineering, University of Tehran, Tehran, Iran
[c] Center of Excellence in Electrochemistry, School of Chemistry, College of Science, University of Tehran, Tehran, Iran
[d] Biosensor Research Center, Endocrinology and Metabolism Molecular-Cellular Sciences Institute, Tehran University of Medical Sciences, Tehran, Iran

ARTICLE INFO

Article history:
Received 5 August 2018
Received in revised form 30 October 2018
Accepted 12 November 2018
Available online 15 November 2018

Keywords:
Gold nanoclusters
Citrate
Paper based
Biomarker

ABSTRACT

Citrate is currently considered a preferred biomarker for the early stage detection of prostate cancer. In the present work, based on the highly efficient catalytic properties of gold nanoclusters, a novel system for optical determination of citrate was successfully established under optimized conditions. Cysteine-capped gold nanoclusters (Cys-AuNCs) are shown to have an intrinsic peroxidase-mimetic activity. In the presence of H_2O_2, Cys-AuNCs nanostructures are able to catalyse the oxidation of 3,3′,5,5′-tetramethylbenzidine (TMB) with high efficiency to produce a blue dye (with an absorbance maximum at 650 nm). Citrate has carboxylic and hydroxyl groups that can bind with free amino and free carboxyl cysteine groups via hydrogen bonds, thus creating a coating on the surface of the gold nanocluster and inhibiting the cluster oxidation activity. Accordingly, a visual, sensitive and simple colorimetric method using Cys-AuNCs as peroxidase mimetic was developed for detecting citrate. A suitable linear relationship for citrate was obtained for the range of 0.5 to 1000 μM. The limit of detection (LOD) of the proposed method was calculated as 0.1 μM and the relative standard deviation (RSD) was obtained to be less than 4.0%. Moreover, the biosensor was used to perform a paper assay on a Y-shaped microfluidic device and make use of the distinctive features of microchannels such as short response time, very low reagent volume required, low fabrication cost etc. A detection limit of 0.4 μM was achieved through the paper test and a good linear range was observed between 1.0 μM–10 mM. The proposed method was further applied to citrate detection in the human urine sample.

1. Introduction

Prostate cancer is among the most common diseases affecting not only Western men but also men in most developing countries since these countries have adapted to such way of living which prevent them from a healthy diet. The fact that there have not been non-invasive nor early stage warning procedures is considered as a serious restriction in diagnosis. In clinical practice, the early diagnosis of prostate cancer is the key factor in reducing mortality rates associated with it; however, very few specific symptoms emerge in the early stages. As a result of the highly specialized anatomical citrate function inside the prostate gland, citrate is currently considered as a selective biomarker for the diagnosis of prostate cancer. The drastic change in citrate levels during the progression of prostate cancer provides a great opportunity for the diagnosis of this type of cancer even in its earliest stages [1]. Citrate levels existing in the human serum have concentrations ranging from 0.06 to 0.14 mM. While, they average 25.4 to 28.9 mM in seminal fluid samples among healthy males. However, these levels are so much lower for the people diagnosed with prostate cancer. As a result, citrate is a viable early marker for prostate cancer diagnosis, providing important information for patient investigation in clinical settings [2]. The estimation of citrate obtained either from prostate or seminal fluid samples may not only be helpful in the investigation of early stage risks but can also be an indicator of the stage, location, and tentative form of the malignancy. Furthermore, the estimation of citrate level can be helpful in the other stages as well, such as disease progression follow-up and regression of the malignancy.

Different analytical approaches, including ion-exchange chromatography [3], HPLC-UV [4], HPLC potentiometry [5], Fluorimetry [6], spectrophotometry [7], chemiluminescence [8], potentiometry [9], mass spectrometry [10], cyclic voltammetry [11], square wave voltammetry [12], amperometry [13], magnetic resonance spectroscopy [14], have been used so far, in order to detect citrate. Electrochemical sensors

* Corresponding author.
E-mail address: smhosseini@khayam.ut.ac.ir (M. Hosseini).

https://doi.org/10.1016/j.saa.2018.11.026
1386-1425/

fabricated by modified electrodes are promising sensing systems to be used as point-of-care diagnosis devices [15,16].

Although all of the aforementioned methods are sensitive, they need expensive and sophisticated equipment, complicated sample preparation, while having time-consuming steps. Therefore, development of new, sensitive, fast, and inexpensive methods is still of great importance in detection of citrate. In comparison with the methods mentioned above, the colorimetric methods are simpler and can be implemented in real-time by even the naked eye or a simple spectrophotometer. Furthermore, the use of microfluidic paper-based analytical devices (μPADs), which possess unique features including low fabrication cost, simplicity, portability and passive movement of the fluids due to capillary action, can be a novel breakthrough for fabrication of simple sensing devices.

These promising platforms have shown great potential in the development of point-of-care Diagnostics. This concept was first proposed by the Whitesides group in 2007 and since then, a variety of methods have been proposed to fabricate microchannels [17].

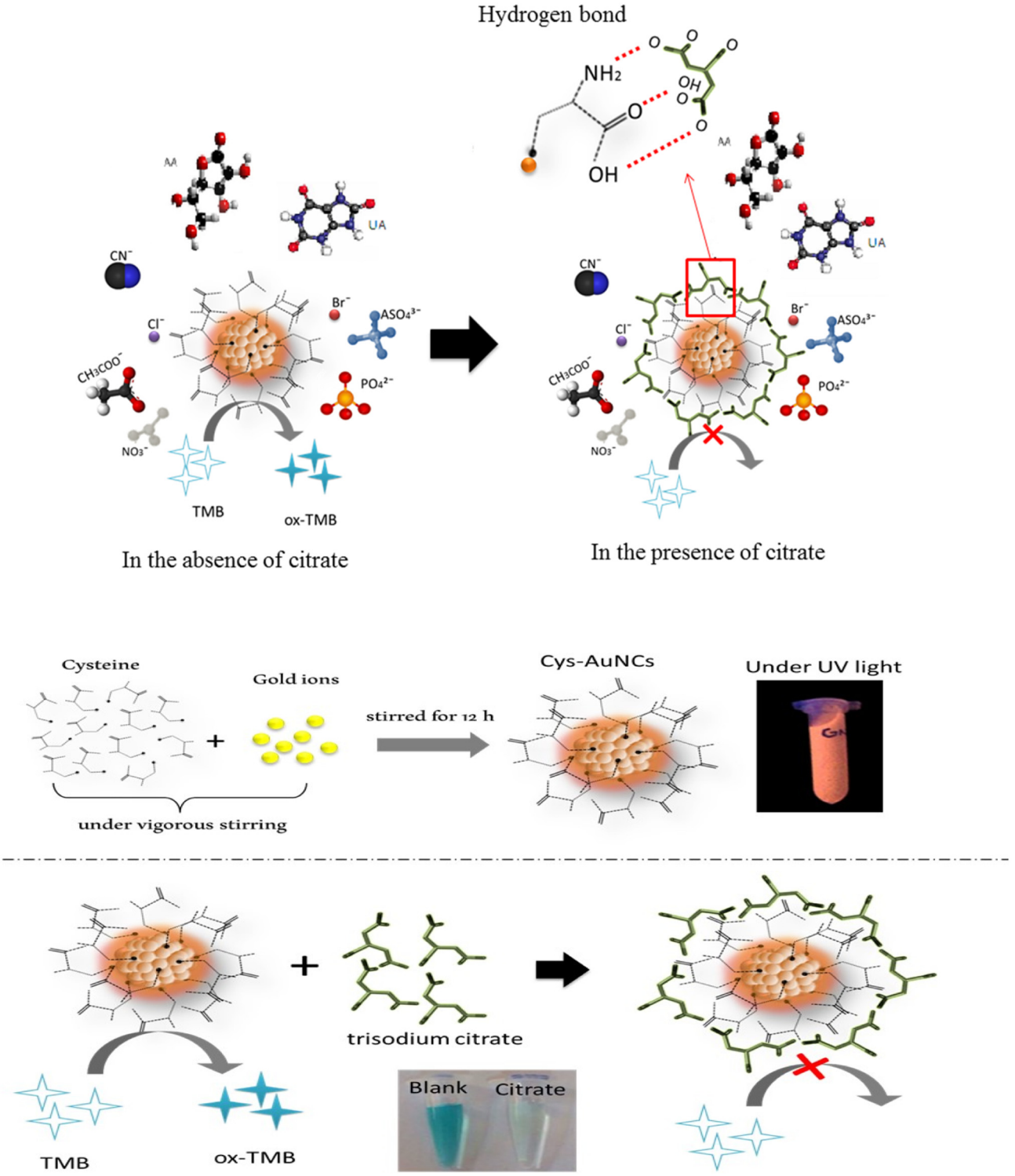

Scheme 1. Principles of citrate detection using Cys-AuNCs as peroxidase mimic.

Cellulose, the most abundant biopolymer on earth, is composed of a network of hydrophilic cellulose fibers. Paper can be considered as a natural cellulose porous microstructure making it a suitable platform for lateral flow via capillary action. Since paper is a hydrophilic platform, hydrophobic barriers are required to confine the fluid flow within a desired section. A number of techniques, including photolithography, wax printing, screen-printing, plasma treating, and laser treating have been developed for the manufacture of hydrophobic barriers [17].

One of the most popular colorimetric sensing strategies is based on the enzymatic transformation of chromogenic substrates, such as TMB to form colorful products in the presence of H_2O_2 [18–23]. Metal nanoclusters show appropriate characteristics thanks to not only their elaborate regulation in nanometer dimensions but also their excellent biocompatibility and low toxicity [24–30] Moreover, in light of having such characteristics as unique optical properties, good water solubility, and excellent stability, the gold nanocluster has received more attention in particular [31–35]. In fact, it has been found that TMB is catalyzed by the gold nanocluster in the presence of H_2O_2, changing the solution color to blue. Consequently, the inherent peroxidase-like activity of such materials as gold nanoclusters is used in order to develop several colorimetric methods. So far, the gold nanocluster peroxidase activity has been used in the detection of certain molecules such as cysteine, ions, and cancerous cells.

In this study, in order to detect citrate ions, which are used in the diagnosis of prostate cancer as well as determination of prostate tumor stages, a novel colorimetric sensor has been developed based on gold nanoclusters (Scheme 1). Despite the fact that the complex role of citrate has not been fully established yet, citrate concentration in the seminal fluid has been found to be proportional to that in the prostate fluid. Hence, the estimation of citrate level has the potential to provide important information, such as disease risk estimation, for patient assessment in multiple clinical settings. It could also be used in early stage diagnosis and prostate malignancy screening tests [36].

2. Experimental

2.1. Apparatus

In order to record the absorbance spectra, the UV–Vis tests were performed by using a Perkin-Elmer lambda25 spectrometer. In addition, a KYKY-EM3200 Transmission Electron Microscopy (TEM) was used to obtain the size and morphology of the NCs.

2.2. Materials and Reagents

All chemicals were either of analytical grade or the highest available quality. Chloroauric acid ($HAuCl_4$ 99.9%), Cysteine, and TMB were purchased from Sigma Aldrich, while Sodium hydroxide (NaOH), hydrochloric acid (HCl) were purchased from Merck. In addition, hydrogen peroxide (H_2O_2), citrate and other anions, Uric acid (UA), Glutathione (GSH), Ascorbic acids (AA) and amino acids including Phenylalanine (Phe), Asparagine (Asn), Histidine (His), Glutamine (Gln), Proline (Pro), Tryptophan (Trp) and Tyrosine (Tyr) used in the selectivity test were purchased from Merck.

2.3. Synthesis of Cys-AuNCs

0.5 mL of a 0.01 M $HAuCl_4$ solution was added to 1.0 mL of fresh Cysteine solution while the solution was being stirred leading to a milky state. Afterwards, the resulting solution was kept under stirring in a 37 °C water bath overnight. The resulting solution was kept at 4 °C for further use. The solution will be stable for 180 days if it is kept under the aforementioned conditions.

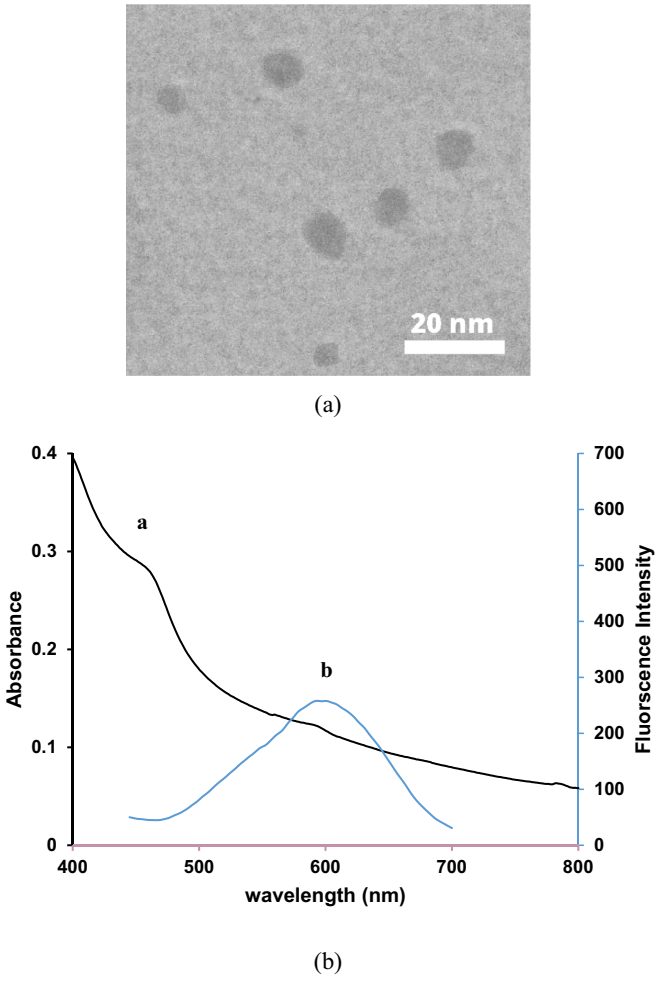

Fig. 1. (a) TEM image and (b) UV–Vis absorption (a) and fluorescence spectra (b) of Cys-AuNCs.

2.4. Citrate Detection Using AuNCs as Peroxidase Mimic

A typical colorimetric analysis for citrate was conducted as follows. First, 50 μL of AuNCs, 70 μL of TMB (10 mM) and 50 μL of H_2O_2 (10 mM) were added to 50 μL of citrate ions with different concentrations (ranging from 0.5 μM–1000 μM). Next, the mixed solution was incubated at room temperature for 10 min and finally, the resultant

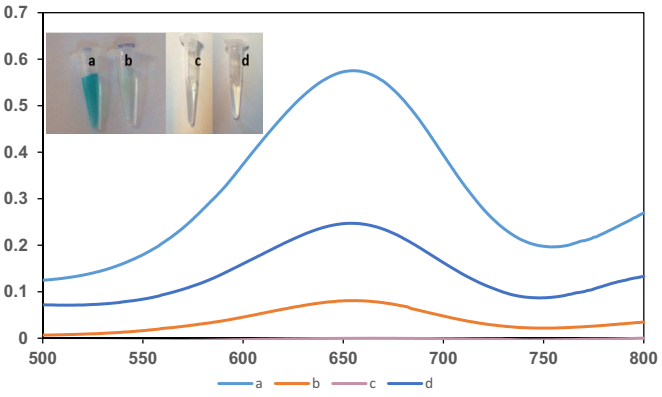

Fig. 2. (A) Different color changes and (B) UV–vis absorption spectra of different reaction systems. (a) Cys-AuNCs-TMB- H_2O_2, (b) Citrate-Cys- AuNCs-TMB- H_2O_2, (c) Cys-AuNCs - TMB and (d) TMB- H_2O_2.

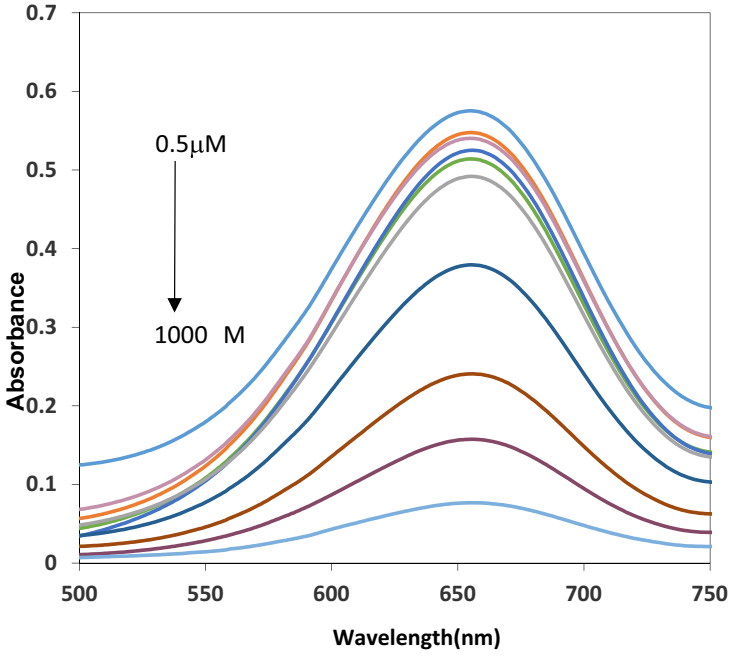

a

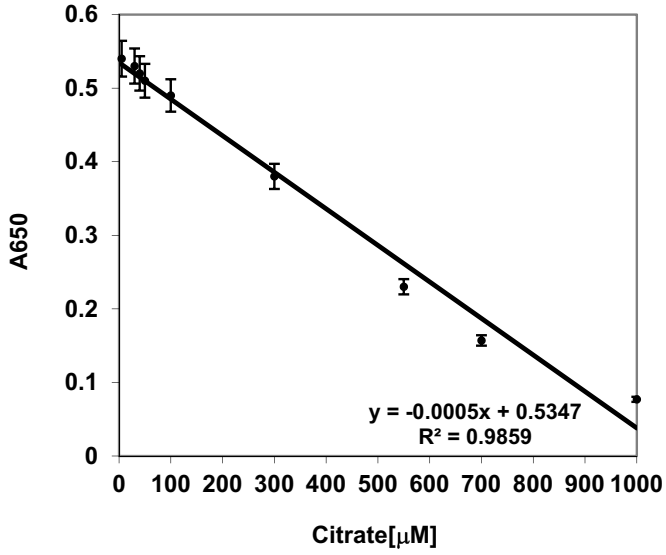

b

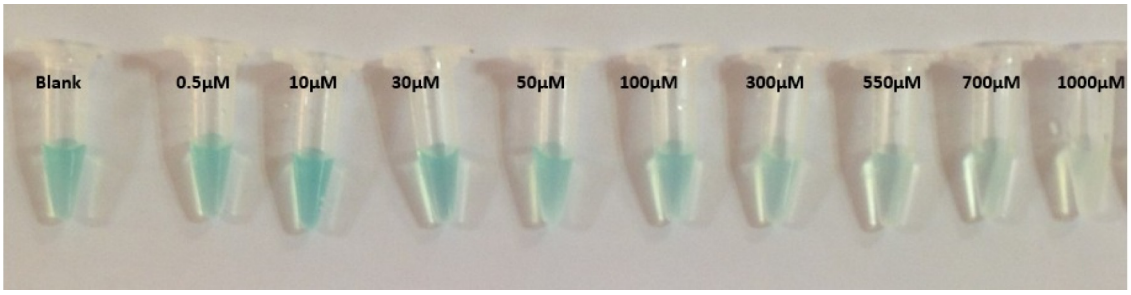

c

Fig. 3. (a) Absorbance spectra of catalytic activity of Cys-AuNCs with TMB and H_2O_2 in the presence of different concentrations of citrate. (b) The peak absorbance change of 650 nm is linear with citrate concentrations (0.5–1000 μM). (c) Color variation in the presence of different concentrations of citrate. The error bars represent the standard deviation of the three measurements.

Table 1
Performance stats of some of citrate colorimetric and fluorescence sensors reported in the literature.

Technique	Interfaces and methods	Detection limit (M)	Linear range (M)	References
Spectrophotometry	Treatment of citrate with metal and $K_2Cr_2O_7$	–	$(4–30) \times 10^{-5}$	[7]
Spectrophotometry	Reduction of Fe^{3+} by citrate upon irradiation with Visible or UV light	2.60×10^{-6}	$(5.21–6.25) \times 10^{-6}$	[46]
Spectrophotometry	Determination of citrate based on the use of citrate lyase and MDH	5.21×10^{-6}	$(5.21–104) \times 10^{-6}$	[47]
Spectrophotometry	Guanidinium Synthetic Receptor/Polyester substrate	4.83×10^{-4}	$(7.79–250) \times 10^{-4}$	[48]
Fluorimetry	Heating a solution of citric acid and *o*-ATH	–	$(2.60–364) \times 10^{-5}$	[6]
Colorimetric	Determination of citrate based on gold nanoclusters catalytic activity	1.0×10^{-7}	5.0×10^{-7}- 1×10^{-3}	This work

DAP: 2,4-diaminophenol.
o-ATH: *o*-aminothiophenol.
MDH: malate dehydrogenase.

solution was used for both adsorption spectroscopy measurement and paper test analysis.

2.5. Paper-based Microfluidic Biosensor Fabrication

The paper-based microfluidic device was fabricated by cutting the Whatman filter No.1 with a CO_2 laser cutter engraver. In order to prevent impurities, which could alter the results due to the interference effect, papers were soaked in distilled water for 1 day after being cut. Then, PVC sheets were used to prevent leaking from the bottom of the channels and reduce the amount of reagent used in the sensing device.

To perform the sensing test, first, 3 μL of AuNCs was immobilized on the two spot zones by simple physical adsorption on paper, carried out by pouring AuNCs on the bare Whatman No.1 microfluidic platform and was left to dry at room temperature. Afterwards, 3 μL of the citrate containing sample was introduced to the right spot zone. In the end, after

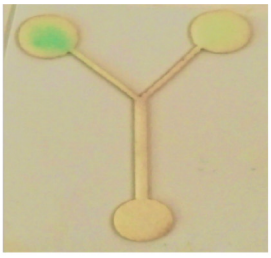

a

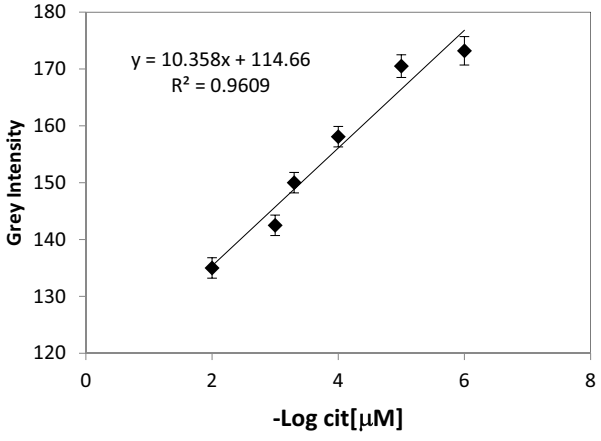

b

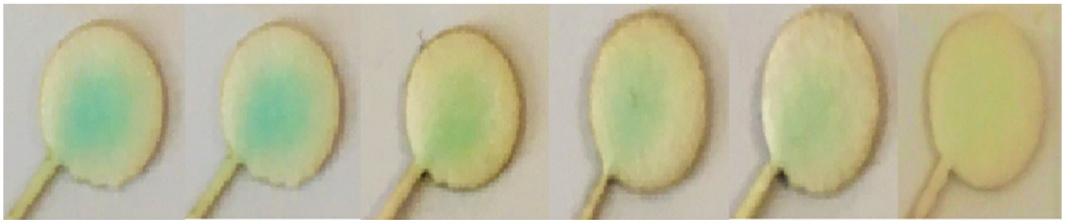

c

Fig. 4. Analytical results of the paper-based device; (a) Paper based microfluidic platform used for the detection of 1 mM citrate solution. (b) Different colors related to different concentrations of citrate ion over the range of 1 μM to 10 mM (c) Detection on the paper-based platform linearly changes from 1 μM to 10 mM of citrate ion concentration.

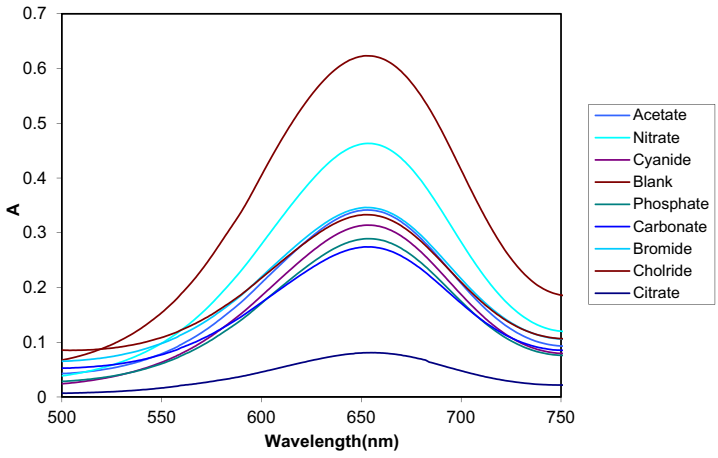
A
Wavelength(nm)
Acetate
Nitrate
Cyanide
Blank
Phosphate
Carbonate
Bromide
Cholride
Citrate

a

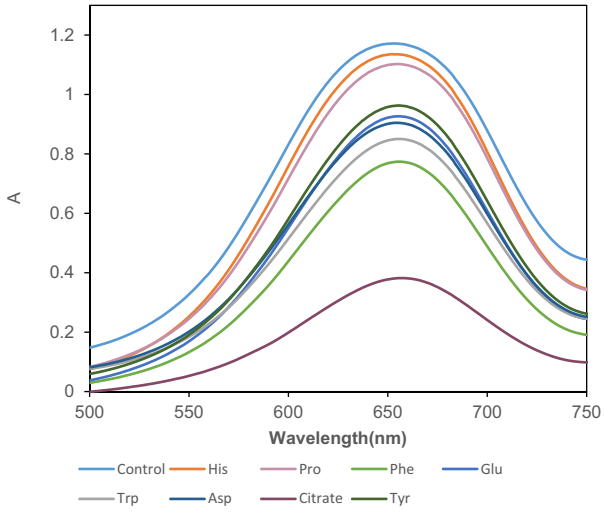
A
Wavelength(nm)
Control
His
Pro
Phe
Glu
Trp
Asp
Citrate
Tyr

b

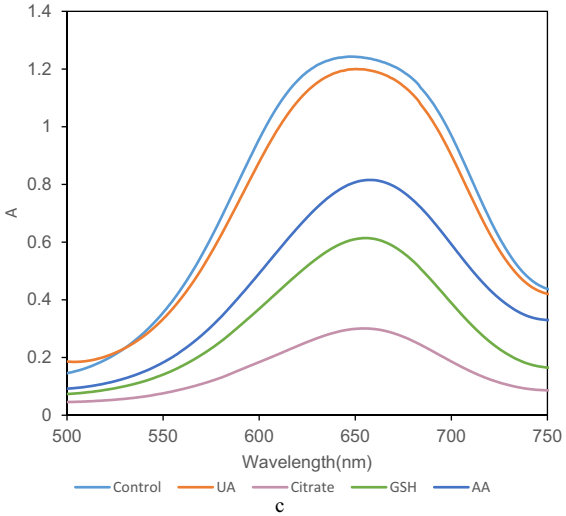
A
Wavelength(nm)
Control
UA
Citrate
GSH
AA

c

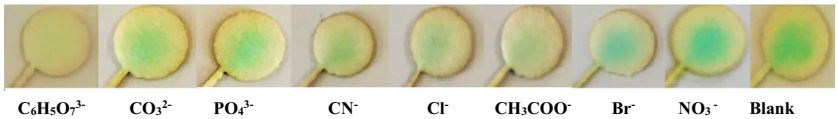
C6H5O7 3-
CO3 2-
PO4 3-
CN-
Cl-
CH3COO-
Br-
NO3 -
Blank

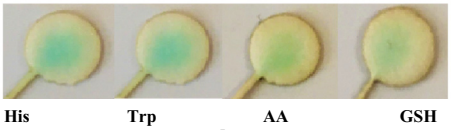
His
Trp
AA
GSH

d

the paper was dried completely, 3 μL of both TMB (10 mM) and H_2O_2 (10 mM) were inserted from the entrance labeled at the bottom of the μPAD. The color of the right side spot zone changed as soon as the mixture of TMB and H_2O_2 reached that area, with its color change distinguishable from the left side spot zone by naked eye. However, at very low concentrations, it was difficult to ascertain the color change. Thus, the Image J software was used for quantitative analysis.

3. Results and Discussion

3.1. Characterization of the Cys-capped AuNCs

It has been shown by recent studies that a thiol group existing in cysteine, could result in a strong complex formation with metal ions. The reason that these complexes were formed strongly was the ability of the thiol group in stabilizing the as-synthesized metal NCs upon the metal sulfur chemistry [37,38]. More evidence obtained by transmission electron microscopy (TEM) indicated that orange emitting Cys-AuNCs was formed. In addition, as can be seen in Fig. 1, the synthesized AuNCs dispersion is very good and they have mostly a diameter between 4 and 6 nm. To characterize the optical properties of the Cys-AuNCs, UV–Vis absorption and fluorescence spectra was carried out. As shown in Fig. 1b the emission of Cys-CuNCs exhibited a peak at approximately 630 nm for 0.01 M concentration of Cys.

3.2. Peroxidase-like Activity of Cys-AuNCs

As can be seen in Fig. 2a, the oxidation of TMB by H_2O_2 could be catalyzed by Cys-AuNCs, resulting in a bright blue product as well as an intense absorption peak at 650 nm in a certain period of time. As expected, the oxidation of TMB in the presence of H_2O_2 was very slow (Fig. 2c). As shown in Fig. 2c, TMB was colorless and displayed no absorbance in the presence of H_2O_2. However, the introduction of Cys-AuNCs to the TMB - H_2O_2 solution catalyzed the reaction, which demonstrates the oxidase property of AuNCs (Fig. 2d). The solution exhibited a deep blue color and a maximum absorption peak at around 650 nm, which results from the oxidation products of TMB. The nanoclusters can break up the O—O bond of H_2O_2 and increase ·OH Radicals. The ·OH radicals are highly oxidative so that they can easily oxidize the colorless TMB. This result indicates that the Cys-AuNCs as the former BSA- AuNCs [39,40], AuNCs [41], Au@Pd [42] and copper nanoclusters [43] behave like peroxidase toward typical peroxidase substrates. The weak absorption was observed only in the case that citrate was added to the Cys-AuNCs solution after introducing TMB and H_2O_2 to the system (Fig. 2b). These results were in agreement with the fact that citrate can serve as an inhibitor of the peroxidase-like activity of Cys-AuNCs.

To determine whether the mixture of TMB, H_2O_2 and Cys-AuNCs is a good platform for citrate detection, the color change of this mixture was investigated in the presence of citrate. As can be seen in Fig. 2, the absorbance spectra of the mixture decreased significantly as citrate was added. The UV–vis spectra of Cys-AuNCs in the presence and absence of citrate are shown in Fig.S1. In the presence of citrate anions, the typical absorbance of Au around of 450 nm is decreased, that can be because of the interaction of citrate anions and Cys-AuNCs. In addition, the FT-IR spectroscopy of compounds was investigated to confirm the attachment of citrate on the Cys-AuNCs surfaces. For citrate, the characteristic bands (centre of gravity at 1417 cm^{-1}) correspond to the symmetric stretching of —COO^-, at 1592 cm^{-1} for the antisymmetric stretching of —COO^-, and at 3455 cm^{-1} due to stretching vibration of —OH, are clearly shown in Fig. S2. When the citrate interacts with Cys-AuNCs (Fig. S2 the antisymmetric stretching of COO^- at 1595 cm^{-1} almost remain same but three new peaks (1331, 1379 and 1485 cm^{-1}) appear on Cys-AuNCs, in addition to citrate, which are symmetric stretching of —COO^- and can be due to the intramolecular interaction between Cys-AuNCs and citrate. Also, A characteristic vibration (C═O) peak of COOH hydrogen bond at 1727 cm^{-1} is observed in the Cys-AuNCs that with addition of citrate is shifted to 1720 cm^{-1}, which is assigned to the formation of intramolecular interaction. It can be suggested that the hydrogen bonds between free carboxyl cysteine groups and carboxylic and hydroxyl citrate groups creates a coating on the surface of the gold nanocluster, thereby inhibiting cluster oxidation activity [44,45]. This observation proves that this platform can be applicable in citrate detection.

3.3. Optimization of Detection Conditions

It is clear that the reaction time and volume of gold nanocluster, TMB, and hydrogen peroxide affect the analytical performance of the sensing system. To accomplish optimal conditions, different volumes of gold nanocluster, TMB, and hydrogen peroxide were utilized. First, various amounts of gold nanocluster including 10, 30, 50, and 70 μL were blended with TMB and hydrogen peroxide. After the resultant solution remained at room temperature for 10 min, it was discovered that the 50 μL gold nanocluster sample led to the highest responding peak. Then, to find the optimal amount of TMB and H_2O_2, different volumes of them (ranging from 10 to 70 μL) were used, and it was discovered that 70 μL of TMB and 50 μL of H_2O_2 led to the highest responding peaks.

In this work, the effect of time on the sensing system was assessed since the reaction time is a significant factor in the colorimetric detection performance. It was found that up to 10 min, absorbance increased with incubation time and started decreasing afterwards. A longer incubation time allows more TMB molecules to react with H_2O_2, but it also increases the duration of experiments. Therefore, the most appropriate time of incubation was determined to be 10 min.

The effect of pH on biosensor performance was also investigated by testing citrate solutions with different pH values (ranging from 4 to 8). It was obtained that at the pH of 6, the nanocluster exhibits the best color change after the addition of TMB and H_2O_2. By increasing the pH, H_2O_2 could decompose into H_2O and O_2 rather than ·OH Radicals causing a decline on oxidation of TMB which has been reported for other nanomaterials with peroxidase-like activity.

3.4. Analytical Performance of the Peroxidase Mimetic Platform for Citrate Detection

In order to assess the catalysis mechanism, different concentrations of citrate were blended with Cys-AuNCs followed by the addition of TMB and H_2O_2. It was observed that as the concentration of citrate increased, the blue color intensity decreased (Fig. 3).

Here, the blueness of oxidized TMB diminished as citrate was introduced, exhibiting the inhabitation impact of citrate on the oxidizing nature of H_2O_2. By using this idea, a fast and simple colorimetric method was developed in order to detect citrate, sensitively. The UV–visible spectra and naked eye color change of oxTMB, which was catalyzed by Cys-AuNCs in the presence of different concentrations of citrate (ranging from 0.5–1000 μM), are depicted in Fig. 3. The values of absorbance at 650 nm are plotted versus citrate concentrations in Fig. 3b, showing a linear trend ranging from 0.5–1000 μM. Moreover, the detection limit and the correlation coefficient were calculated to be 0.1 μM and $R^2 = 0.9859$, respectively.

Different analytical devices using various spectroscopy methods have been utilized so far for the detection of citrate ions. Table 1 compares the result of these devices with our colorimetric method, showing a better performance of our biosensor in terms of the dynamic linear range and lower detection limit.

Fig. 5. Selectivity of the citrate biosensor against other ions (CN^-, Cl^-, NO_3^-, CO_3^{2-}, Br^-, CH_3COO^-, PO_4^{3-}, and $C_6H_5O_7^{3-}$) (a), amino acids (His, Pro, Phe, Gln, Trp, Asn, Tyr and Citrate) (b) and other biomolecule (AA, UA, GSH) (c) with the same cationic concentration (1000 μM)). (d) paper-based selectivity test.

3.5. Analytical Performance of the Microfluidic Aptasensor on μM Device

Paper-based biosensors are good choices for assays, as they require low sample volumes and shorter sensing procedure time. Therefore, they are used for the detection of different targets. The paper-based biosensor used in this research and its corresponding color change is depicted in Fig. 4a. It can be seen that as the concentration of citrate increases, the right spot color changes, and its whiteness gradually turns into blueness. Hence, the blue intensity increases (detected by the naked eye), owing to the hindrance effect of citrate. The Image J software was used to measure the citrate level, quantitatively. As can be seen in Fig. 4b, the biosensor shows a good linear range ($y = 10.358\ x + 114.66$, $R^2 = 0.9609$) in the range of 1.0 μM–10 mM. In other words as citrate concentration increases, the grey intensity of right spot zone decreases. The detection limit of the biosensor was measured to be 0.4 μM, Which was an acceptable one since the normal citrate concentration in urine samples is about 2 mM or less with men diagnosed with prostate cancer [17].

3.6. Selectivity

One of the most important characteristics of a detection device is its ability to detect the target selectively. To assess this, different anions, including CN^-, Cl^-, NO_3^-, CO_3^{2-}, Br^-, CH_3COO^-, PO_4^{3-}, and $C_6H_5O_7^{3-}$, were tested both in the solution and on μPADs, in the same condition where the citrate was tested. Fig. 5(a–d) shows that the addition of ions other than citrate did not lead to a significant change in the blueness of the solution. As shown in Fig. 5b, amino acids including Phe, Asn, His, Gln, Pro, Trp and Tyr and other biomolecules (Fig. 5c) such as AA, UA did not cause obvious changes in absorbance of solution at 650 nm except of GSH that has a slightly interference on this inhibition effect. However, the citrate addition made the solution less blue implying that our device is able to detect citrate ions selectively.

3.7. Application in Urine Analysis

In order to investigate the ability of the nano-biosensor in the detection of real samples, it was used to detect citrate in urine samples. To do so, a healthy volunteer's fresh urine sample was used. First, the concentration of citrate was determined through Lyase enzyme-colorimetric method (data were provided by Noor Pathobiology Laboratory). After that, four different concentrations of the citrate solution were made out of the aforementioned urine sample. The samples were centrifuged at 3000 rpm for 5 min, and the free supernatant was withdrawn by a pipette. Afterwards, the supernatant was filtered by using a 0.2 μm syringe filter. In order to evaluate our method, a four-time diluted urine sample was introduced to the biosensor.

For each sample, citrate concentration was calculated by both the Cys-AuNCs biosensor and Lyase enzyme-colorimetric method (Table 2). As can be seen, the recovery of the present biosensor, ranging from 86.0% to 98.0% ($n = 3$), shows a satisfactory result. The results show that citrate presence can be precisely detected, meaning that our method is applicable for detection of complex biological samples.

By comparing the aforementioned results, it is obvious that our sensing device can be applied practically to detect citrate in biological samples (Table 2). The price and simplicity of a portable sensor should be considered in fabrication steps. Although the nanocluster or multifactor dependent process raises the cost of the system, its sensitivity is another factor that should be taken into account. In fact, although some of the methods reported by other researchers have achieved low detection limits, our device has such a low detection limit that it can detect normal thresholds of citrate in all biological fluids, such as urine, at much lower costs.

Table 2
Analytical results for citrate in human urine samples using the proposed method and the Lyase enzyme-colorimetric method.

Sample	Lyase enzyme-colorimetric method (μM)	Cys-AuNCs biosensor (μM)	Recovery (%)
1	100	86.0 (±1.2)	86.0
2	500	450.0 (±6.0)	90.0
3	1000	880.0 (±8.0)	88.0
4	5000	4900.0 (±10.0)	98.0

4. Conclusion

In summary, we have demonstrated a simple, convenient, and sensitive strategy for the detection of citrate with the naked eye, both in solutions and on μPADs. One of the most prominent features of this sensing system is that the Cys-AuNCs were directly used to detect citrate ions without modification. The second significant feature of this study is that a novel paper-based colorimetric method for ultrasensitive detection of citrate ions was developed, which induced a color change of the tested solution from blue to colorless. This method presents good sensitivity and appears to be a promising device for practical applications.

Acknowledgments

The authors thank the research Council of University of Tehran (Grant 28645/01/02) for financial support of this work.

Appendix A. Supplementary Data

Supplementary data to this article can be found online at https://doi.org/10.1016/j.saa.2018.11.026.

References

[1] N. Liu, Z. Gao, H. Ma, P. Su, X. Ma, X. Li, G. Ou, Simultaneous and rapid detection of multiple pesticide and veterinary drug residues by suspension array technology, Biosens. Bioelectron. 41 (2013) 710–716.
[2] S. Azzouzi, H.K. Patra, M.B. Ali, M.N. Abbas, C. Dridi, A. Errachid, A.P.F. Turner, Citrate-selective electrochemical μ-sensor for early stage detection of prostate cancer, Sensors Actuators B Chem. 228 (2016) 335–346.
[3] B.M. Deborba, J.S. Rohrer, L. Bhattacharyya, Development and validation of an assay for citric acid/citrate and phosphate in pharmaceutical dosage forms using ion chromatography with suppressed conductivity detection, J. Pharm. Biomed. Anal. 36 (2004) 517–524.
[4] R. Scherer, A.C.P. Rybka, C.A. Ballus, A.D. Meinhart, J. Teixeira Filho, H.T. Godoy, Validation of a HPLC method for simultaneous determination of main organic acids in fruits and juices, Food Chem. 135 (2012) 150–154.
[5] Z.L. Chen, D. Hibbert, Simultaneous amperometric and potentiometric detection of sugars, polyols and carboxylic acids in flow systems using copper wire electrodes, J. Chromatogr. A 766 (1997) 27–33.
[6] M. Hori, T. Kometani, H. Ueno, H. Morimoto, A new fluorometric analysis of citric acid, Biochem. Med. 11 (1974) 49–59.
[7] A.S. Pérez, J.H. Mendez, J.G. Bárez, Polarographic and spectrophotometric determination of citrate in commercial orange and lemon drinks, Food Chem. 32 (1989) 69–79.
[8] H. Zhike, G. Hua, Y. Liangjie, L. Shaofang, M. Hui, L. Xiaoyan, Z. Yun'e, Pulse injection analysis with chemiluminescence detection: determination of citric acid using tris-(2, 2′-bipyridine) ruthenium (II), Talanta 47 (1998) 301–304.
[9] C.L. Araújo, E.I. Melo, N.M. Coelho, Potentiometric detection of citrate in beverages using a graphite carbon electrode, Talanta 84 (2011) 1169–1173.
[10] A. Ghassempour, N.M. Najafi, A.A. Amiri, Determination of citric acid in fermentation media by pyrolysis mass spectrometry, J. Anal. Appl. Pyrolysis 70 (2003) 251–261.
[11] S. Awasthi, A. Srivastava, M. Singla, Voltammetric determination of citric acid and quinine hydrochloride using polypyrrole–pentacyanonitrosylferrate/platinum electrode, Synth. Met. 161 (2011) 1707–1712.
[12] S. Azzouzi, M.B. Ali, M.N. Abbas, J. Bausells, N. Zine, A. Errachid, Novel iron (III) phthalocyanine derivative functionalized semiconductor based transducers for the detection of citrate, Org. Electron. 34 (2016) 200–207.
[13] K. Matsumoto, T. Tsukatani, Y. Okajima, Amperometric flow-injection determination of citric acid in food using free citrate lyase and co-immobilized oxalacetate decarboxylase and pyruvate oxidase, Electroanalysis 7 (1995) 527–530.
[14] G.M. Villeirs, W. Oosterlinck, E. Vanherreweghe, G.O. De Meerleer, A qualitative approach to combined magnetic resonance imaging and spectroscopy in the diagnosis of prostate cancer, Eur. J. Radiol. 73 (2010) 352–356.
[15] H. Beitollahi, I. Sheikhshoaie, Electrocatalytic oxidation and determination of epinephrine in the presence of uric acid and folic acid at multiwalled carbon

nanotubes/molybdenum (VI) complex modified carbon paste electrode, Anal. Methods 3 (2011) 1810–1814.
[16] H.-B. Wang, H.-D. Zhang, Y. Chen, Y.-M. Liu, A fluorescent biosensor for protein detection based on poly (thymine)-templated copper nanoparticles and terminal protection of small molecule-linked DNA, Biosens. Bioelectron. 74 (2015) 581–586.
[17] S. Liu, W. Su, X. Ding, A review on microfluidic paper-based analytical devices for glucose detection, Sensors 16 (2016) 2086.
[18] C. Wu, D. Fan, C. Zhou, Y. Liu, E. Wang, Colorimetric strategy for highly sensitive and selective simultaneous detection of histidine and cysteine based on G-quadruplex-Cu (II) metalloenzyme, Anal. Chem. 88 (2016) 2899–2903.
[19] M. Rahimi-Nasrabadi, F. Mizani, M. Hosseini, A. Homayoun Keihan, M.R. Ganjali, Detection of hydrogen peroxide and glucose by using $Tb_2(MoO_4)_3$ nanoplates as peroxidase mimics, Spectrochim. Acta A Mol. Biomol. Spectrosc. 186 (2017) 82–88.
[20] Y.S. Borghei, M. Hosseini, M.R. Ganjali, Visual detection of miRNA using peroxidase-like catalytic activity of DNA-CuNCs and methylene blue as indicator, Clin. Chim. Acta 483 (2018) 119–125.
[21] M. Hosseini, M. Aghazadeh, M.R. Ganjali, A facile one-pot synthesis of cobalt-doped magnetite/graphene nanocomposite as peroxidase mimetics in dopamine detection, New J. Chem. 41 (2017) 12678–12684.
[22] M. Hosseini, F.S. Sabet, H. Khabbaz, M. Aghazadeh, F. Mizani, M.R. Ganjali, Enhancement of the peroxidase-like activity of cerium-doped ferrite nanoparticles for colorimetric detection of H_2O_2 and glucose, Anal. Methods 9 (2017) 3519–3524.
[23] H.-B. Wang, Y. Li, G.-L. Dong, T. Gan, Y.-M. Liu, A convenient and label-free colorimetric assay for dopamine detection based on the inhibition of the Cu (ii)-catalyzed oxidation of a 3, 3′, 5, 5′-tetramethylbenzidine–H_2O_2 system, New J. Chem. 41 (2017) 14364–14369.
[24] H.C. Yeh, J. Sharma, J.J. Han, J.S. Martinez, J.H. Werner, A DNA— silver nanocluster probe that fluoresces upon hybridization, Nano Lett. 10 (2010) 3106–3110.
[25] Y.S. Borghei, M. Hosseini, M.R. Ganjali, H. Ju, Colorimetric and energy transfer based fluorometric turn-on method for determination of microRNA using silver nanoclusters and gold nanoparticles, Microchim. Acta 185 (2018) 286.
[26] Y.S. Borghei, M. Hosseini, R. Ganjali, S. Hosseinkhani, A novel BRCA1 gene deletion detection in human breast carcinoma MCF-7 cells through FRET between quantum dots and silver nanoclusters, J. Pharm. Biomed. Anal. 152 (2018) 81–88.
[27] Y.S. Borghei, M. Hosseini, M.R. Ganjali, Detection of large deletion in human BRCA1 gene in human breast carcinoma MCF-7 cells by using DNA-silver Nanoclusters, Methods Appl. Fluoresc. 6 (2017), 015001. .
[28] Y.S. Borghei, M. Hosseini, M.R. Ganjali, Synthesis of fluorescent cysteine-gold Nanoclusters (Cys-Au-NCs) and their application as Nano-biosensors for the determination of cysteine, Curr. Nanosci. 13 (2017) 610–615.
[29] C. Wang, J. Li, C. Amatore, Y. Chen, H. Jiang, X.M. Wang, Gold nanoclusters and graphene nanocomposites for drug delivery and imaging of cancer cells, Angew. Chem. Int. Ed. 50 (2011) 11644–11648.
[30] H.-B. Wang, Y. Li, H.-Y. Bai, Y.-M. Liu, DNA-templated Au nanoclusters and MnO_2 sheets: a label-free and universal fluorescence biosensing platform, Sensors Actuators B Chem. 259 (2018) 204–210.
[31] Y.S. Borghei, M. Hosseini, M.R. Ganjali, Fluorometric determination of microRNA via FRET between silver nanoclusters and CdTe quantum dots, Microchim. Acta 184 (2017) 4713–4721.
[32] Y.S. Borghei, M. Hosseini, M.R. Ganjali, S. Hosseinkhani, Label-free fluorescent detection of microRNA-155 based on synthesis of hairpin DNA-templated copper nanoclusters by etching (top-down approach), Sensors Actuators B Chem. 248 (2017) 133–139.
[33] Y.S. Borghei, M. Hosseini, M.R. Ganjali, Fluorescence based turn-on strategy for determination of microRNA-155 using DNA-templated copper nanoclusters, Microchim. Acta 184 (2017) 2671–2677.
[34] M. Hosseini, Y. Ahmadi, S. Borghei, M.R. Ganjali, A new fluorescence turn-on nanobiosensor for the detection of micro-RNA-21 based on a DNA–gold nanocluster, Methods Appl. Fluoresc. 5 (2017) 1015005.
[35] H.A. Kermani, M. Hosseini, M. Dadmehr, M.R. Ganjali, Rapid restriction enzyme free detection of DNA methyltransferase activity based on DNA-templated silver nanoclusters, Anal. Bioanal. Chem. 408 (2016) 4311–4318.
[36] N. Liu, W. Liang, X. Ma, X. Li, B. Ning, C. Cheng, et al., Simultaneous and combined detection of multiple tumor biomarkers for prostate cancer in human serum by suspension array technology, Biosens. Bioelectron. 47 (2013) 92–98.
[37] Y. Negishi, K. Nobusada, T. Tsukuda, Glutathione-protected gold clusters revisited: bridging the gap between gold (I)— thiolate complexes and thiolate-protected gold nanocrystals, J. Am. Chem. Soc. 127 (2005) 5261–5270.
[38] N. Goswami, K. Zheng, J. Xie, Bio-NCs–the marriage of ultrasmall metal nanoclusters with biomolecules, Nanoscale 6 (2014) 13328–13347.
[39] X.-X. Wang, Q. Wu, Z. Shan, Q.-M. Huang, BSA-stabilized au clusters as peroxidase mimetics for use in xanthine detection, Biosens. Bioelectron. 26 (2011) 3614–3619.
[40] G.-L. Wang, L.-Y. Jin, Y.-M. Dong, X.-M. Wu, Z.-J. Li, Intrinsic enzyme mimicking activity of gold nanoclusters upon visible light triggering and its application for colorimetric trypsin detection, Biosens. Bioelectron. 64 (2015) 523–529.
[41] J. Feng, P. Huang, S. Shi, K.-Y. Deng, F.-Y. Wu, Colorimetric detection of glutathione in cells based on peroxidase-like activity of gold nanoclusters: a promising powerful tool for identifying cancer cells, Anal. Chim. Acta 967 (2017) 64–69.
[42] Z. Dehghani, M. Hosseini, J. Mohammadnejad, B. Bakhshi, A.H. Rezayan, Colorimetric aptasensor for *Campylobacter jejuni* cells by exploiting the peroxidase like activity of Au@ Pd nanoparticles, Microchim. Acta 185 (2018) 448.
[43] Z. Yan, Q. Niu, M. Mou, Y. Wu, X. Liu, S. Liao, A novel colorimetric method based on copper nanoclusters with intrinsic peroxidase-like for detecting xanthine in serum samples, J. Nanopart. Res. 19 (2017) 235.
[44] M. Stobiecka, J. Deeb, M. Hepel, Ligand exchange effects in gold nanoparticle assembly induced by oxidative stress biomarkers: Homocysteine and cysteine, Biophys. Chem. 146 (2010) 98–107.
[45] J.W. Park, J.S. Shumaker-Parry, Structural study of citrate layers on gold nanoparticles: role of intermolecular interactions in stabilizing nanoparticles, J. Am. Chem. Soc. 136 (2014) 1907–1921.
[46] E. Luque-Pérez, A. Ríos, M. Valcárcel, Flow-injection spectrophotometric determination of citric acid in beverages based on a photochemical reaction, Anal. Chim. Acta 366 (1998) 231–240.
[47] M. Plantá, F. Lázaro, R. Puchades, A. Maquieira, Determination of citric acid and oxalacetic acid in foods by enzymic flow injection, Analyst 118 (1993) 1193–1197.
[48] L. Capitan-Vallvey, E.A. Guerrero, C.B. Merelo, M.F. Ramos, A test strip for chloride analysis in environmental water, Anal. Bioanal. Chem. 380 (2004) 563–569.